

# Design of an AGV for Improved CDGPS-based Control Performance

Mathieu Joerger, John Christ, Richard Duncan and Boris Pervan  
*Mechanical, Materials and Aerospace Department  
Illinois Institute of Technology*

## BIOGRAPHY

Mathieu Joerger is a PhD student in Mechanical and Aerospace Engineering at the Illinois Institute of Technology (IIT) in Chicago. In 2002, he obtained a Master in Mechatronics at the Ecole Nationale Supérieure des Arts et Industries de Strasbourg (France) and a Master of Science in Mechanical and Aerospace Engineering at IIT. He is currently working as a research assistant on robotic applications involving distributed navigation systems.

John Christ works currently as a Project Engineer. In 1989, he obtained a Bachelors Degree in Engineering Science from Iowa State University in Ames, Iowa and in 2003, a Master of Science Degree in Mechanical and Aerospace Engineering from IIT. His Thesis work at IIT included developing the autonomous ground vehicle and testing the GPS based navigation system.

Richard Duncan is a B.S. student in Aerospace Engineering and Materials and Metallurgical Engineering at IIT. He plans to finish his undergraduate work in the fall of 2005 and continue in graduate work. He is currently working as an undergraduate research assistant in the Navigation and Guidance Lab at IIT focusing on software development and support of hardware testing.

Boris Pervan received a B.S. from the University of Notre Dame (1986), M.S. from the California Institute of Technology (1987), and Ph.D. from Stanford University (1996), all in Aerospace Engineering. From 1987 to 1990, he was a Systems Engineer at Hughes Space and Communications Group. Dr. Pervan was a Research Associate at Stanford from 1996 to 1998, serving as project leader for GPS Local Area Augmentation System (LAAS) research and development. He was the 1996 recipient of the RTCA William E. Jackson Award and the 1999 M. Barry Carlton Award from the IEEE Aerospace and Electronic Systems Society. Currently, Dr. Pervan is Assistant Professor of Mechanical and Aerospace Engineering at IIT where he received the Outstanding Graduate Teaching Award (2002).

## ABSTRACT

This paper introduces and demonstrates a procedure to optimize the path-following performance of an autonomous vehicle system using Differential Global Positioning System (DGPS) navigation. In traditional applications of this type, the navigation, guidance and control system is designed and built for an existing vehicle. In contrast, in this work we carry out an *integrated* design of the vehicle with its controller. The integrated design process is oriented toward directly maximizing the path-following performance, rather than individually optimizing secondary vehicle characteristics such as the operating velocity. Using this method, system performance is maximized, and unnecessary and costly additional equipment or over-sized components can be avoided.

Detailed covariance analyses and closed-loop simulations are carried out to evaluate the ultimate dynamic performance and to quantify the impact of each vehicle parameter. In particular, the performance sensitivity is analyzed with respect to parameters for which no obvious selection criteria exist, such as the vehicle's sense of motion or the positioning sensor location, which prove to be decisive characteristics. Experimental testing on a prototype rover confirms the simulations' results and validates the selection of the vehicle design parameters.

As an example of practical application, the prototype rover is used as an automated lawnmower. The versatile modular design and the flexible parametric control system enable the successful integration of the mower to the vehicle system.

## INTRODUCTION

Automated Ground Vehicles (AGVs) can support a variety of highly-detailed missions that are unsafe or too difficult for human operation. In 1997, O'Connor [1], whose work was later refined by Bell [2], set the path for the development and expansion of DGPS-based automated vehicle control techniques in practical

applications. The critical centimeter-level accuracy provided by Carrier-Phase DGPS (CDGPS) [3] enabled the successful control of a tractor for unmanned agricultural field plowing. Since then, in less than a decade, precision-controlled AGVs have been successfully implemented in outdoor applications such as ramming of ski runs [4], topographic field mapping, handling of hazardous materials, lawn mowing and more [5]. For trajectory-tracking operations of this type, the control performance can be improved by increasing the frequency of the course corrections. Multisensor systems, such as the CDGPS aided inertial navigation system (INS) by Farrell et al. [6], have been implemented in order to obtain higher measurement update rates. But the actuators' dynamic bandwidth needs to be selected accordingly.

In this paper, the relationship between design parameters, including actuator and sensor characteristics, and path-following performance is established, so that vehicle components can be optimally selected. Carefully derived parametric models for both the vehicle and the controller are used in detailed covariance analysis and closed-loop simulations; performance predictions are estimated as functions of design parameters.

To illustrate this idea, we designed, built and tested a prototype AGV called 'Leonard'. Vehicle characteristics, such as the sense of motion, the operating velocity, the positions of the GPS antenna (positioning sensor location) and of the control point (the point on the AGV designated to follow the predefined trajectory) are selected before the rover is built, for a desired trajectory-tracking performance to be achieved. Experimental testing supports the predicted results, confirms the vehicle parameter selection, and validates the design process.

The implementation of Leonard as an automated lawnmower is a practical illustration of the versatility of its mechanical design and of the flexibility of its control system. Again, the analytical design process is used to perform the modifications necessary to the addition of the mower; it is especially relevant for the choice of cutting blades' location.

## BASELINE VEHICLE DESIGN

To provide a simple framework for the vehicle system analysis, we focus on a differential drive AGV concept. Steering is performed by a difference in angular velocity on two opposed driving wheels. Figure 1 gives an overview of the major vehicle components. In this section, the actuators and the aluminum frame's dimensions are pre-selected, because they are subject to mechanical constraints (the vehicle's length and width are limited by the size of the storage area; the actuators'

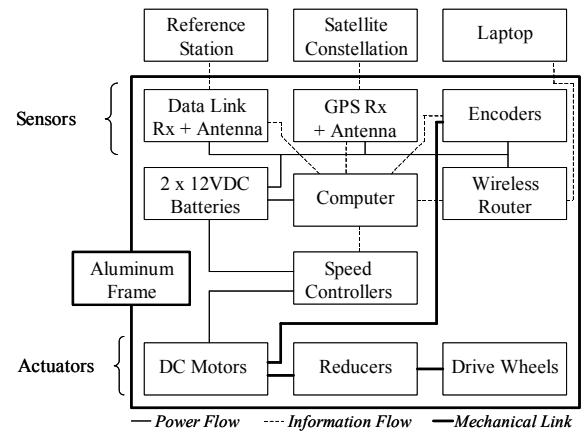


Figure 1 Vehicle Components

selection is dependent on numerous factors such as the weight, and the batteries amperage). However, the positions of the sensor and control points in the final assembly, as well as the operating velocity, the sense of motion and the controller's update rate are selected by analysis in the rest of the paper.

The actuators are composed of two DC-motors with gear-and-belt type reducers linked to the driving wheels. An iterative process is used to confirm that the selected actuators together with their mounting elements (bearing, shafts, sprockets, etc.), selected from the available market supply, can move the weight of the total assembly [7]. The DGPS sensor is composed of a GPS receiver (NovAtel ProPakII) and a spread spectrum data link in communication with the reference station. The GPS patch-antenna is fixed at the center of an aluminum plate in order to minimize the effects of multipath reflections. Optical encoders are mounted on the motor's driving shaft but used only occasionally as an auxiliary sensor during testing.

Sensor data is processed by an embedded computer equipped with a data acquisition card, which sends commands to the motors via speed-controller interfaces. The purpose of the speed controllers is to provide to the motors the necessary amperage at the computer's request. Additionally, a wireless system provides remote-control capability, which is useful for testing. The power is delivered by two 12V-DC batteries, which allow for up to four hours of autonomous operation. All the components with the exceptions of the antennae and the wheels, are enclosed in a water-proof and dust-proof rugged aluminum frame. Two floating casters are added to ensure vehicle balance and stability. Details on the selection of the components are available in reference [7].



$$\omega_{MR} = \frac{N}{R} \left( \dot{x} \sin \phi - \dot{y} \cos \phi - \frac{W}{2} \dot{\phi} \right) \quad (6)$$

$$\omega_{ML} = \frac{N}{R} \left( \dot{x} \sin \phi - \dot{y} \cos \phi + \frac{W}{2} \dot{\phi} \right) \quad (7)$$

and under the assumption (verified for the class of motors selected) that the electromechanical time constant is small with respect to the other time constants, we obtain an equation applicable to the left and right motors:

$$\frac{C_{R/L}}{N} = \frac{k_T}{R_a} u_{R/L} - J \dot{\omega}_{MR/L} - \left( \frac{k_T k_E}{R_a} + f_V \right) \omega_{MR/L} \quad (8)$$

where the parameters are described Table 1.

Finally, the last three equations are combined to the model with torque-inputs. The resulting model is linearized at constant velocity ( $V_{y0}$ ) along a straight line, chosen to be the  $y$ -axis, and therefore assuming a small heading-angle  $\phi$ . Linearization hypotheses are later verified. We eventually obtain a complete linear dynamic model for the vehicle, expressed in matrix form:

$$\begin{bmatrix} \ddot{y} \\ \ddot{\phi} \\ \dot{x} \\ \dot{y} + V_{y0} \\ \dot{\phi} \end{bmatrix} = \begin{bmatrix} \gamma & 0 & 0 & 0 & 0 \\ 0 & \alpha' & 0 & 0 & 0 \\ 0 & -L_A & 0 & 0 & V_{y0} \\ 1 & 0 & 0 & 0 & 0 \\ 0 & 1 & 0 & 0 & 0 \end{bmatrix} \begin{bmatrix} \dot{y} + V_{y0} \\ \dot{\phi} \\ x \\ y \\ \phi \end{bmatrix} + \begin{bmatrix} \zeta & \zeta \\ -\beta' & \beta' \\ 0 & 0 \\ 0 & 0 \\ 0 & 0 \end{bmatrix} \begin{bmatrix} u_R \\ u_L \end{bmatrix} \quad (9)$$

$$\begin{bmatrix} x_s \\ y_s \end{bmatrix} = \begin{bmatrix} 0 & 0 & 1 & 0 & L_S \\ 0 & 0 & 0 & 1 & 0 \end{bmatrix} \begin{bmatrix} \dot{y} + V_{y0} \\ \dot{\phi} \\ x \\ y \\ \phi \end{bmatrix} \quad (10)$$

with:

$$\gamma = -2N^2 \frac{f_V + k_T k_E / R_a}{mR^2 + 2N^2 J} \quad (11)$$

$$\zeta = \frac{RNk_T}{(mR^2 + 2N^2 J)R_a}$$

$$\alpha' = \frac{\alpha R^2 - \beta W N^2 (f_V + k_T k_E / R_a)}{R^2 + \beta N^2 J W} \quad (12)$$

$$\alpha = \frac{m(L_A - L_B)V_{y0}}{J_{ZZ} + m(L_A - L_B)^2} \quad (13)$$

$$\beta = \frac{W}{2(J_{ZZ} + m(L_A - L_B)^2)}$$

$$J_{ZZ} = \frac{1}{12} m(L^2 + W^2)$$

For notation purposes, we re-write the input equation (9) and the output equation (10):

$$\begin{aligned} \dot{\mathbf{x}} &= F\mathbf{x} + G\mathbf{u} \\ \mathbf{y} &= H\mathbf{x} \end{aligned}$$

where  $\mathbf{x}$  is the state vector,  $\mathbf{u}$  is the input vector,  $\mathbf{y}$  is the output vector,  $F$  is the system matrix,  $G$  is the input matrix, and  $H$  is the output matrix. Equations (6) and (7) are linearized and added to the output equation when using encoder measurements of the drive shafts' angular velocities. Note that the representation can be separated into two uncoupled modes representing the in-track ( $\dot{y}$  and  $y$ ) and cross-track ( $\dot{\phi}$ ,  $x$  and  $\phi$ ) motion, the latter being of prime interest.

The study of the vehicle system's open-loop poles, though not ultimately decisive, provides valuable insights into the system's closed-loop performance. Here in particular, vehicle parameters can be selected to make the open-loop poles more stable. Consider first the model with torque inputs, for which  $\alpha$  (13) is the only non-zero pole. If the center of mass ( $B^*$ ) is on the driving axle ( $B^*$  coincident with  $A$ , hence  $L_A - L_B = 0$ ), the system is marginally unstable. If it is not, open-loop stability is a function of the sense of motion, determined by the sign of  $V_{y0}$ . Thus if  $B^*$  is forward from  $A$  in the sense of motion, the system is marginally unstable. With  $B^*$  in the back, it is unstable. This difference in control stability can be given an experimental interpretation by observing the unforced motion of a loaded supermarket cart, which is also a differential-drive type of system. When the center of mass is in the front, the trajectory is smooth. When it is in the back, the cart turns around. For these reasons, we call "forward" motion, the movement of the vehicle when  $B^*$  is in front of the driving axle.

The same open-loop stability analysis is carried out for the system with voltage inputs. In this case there are two non-zero poles,  $\gamma$  (11) for the in-track mode and  $\alpha'$  (12) for the cross-track mode, both of which are functions of motor parameters. For the class of motors considered,  $\gamma$  is always negative. The same is true for  $\alpha'$ , but since it is a function of  $\alpha$ , the pole is more stable in forward motion than in backward motion. The resulting impact on the trajectory-tracking performance is quantified later in this paper.

## DESIGN OF THE CONTROLLER

The design of the navigation, guidance and control system is based on modern control theory and uses the state space representation (9) and (10) derived in the previous section. The control system is a discrete-time closed-loop feedback algorithm using a Linear Quadratic Regulator (LQR) and a Kalman filter. As opposed to traditional methods, the controller's elements must be expressed in terms of vehicle parameters. Indeed, in the next section,

we will analyze the system's responses to variations in these parameter values. The controller must therefore account for changes in the vehicle's configuration, so that systematic comparisons be fair.

The derivation of the optimal LQR control gain is based on the minimization of a cost function of the form:

$$J_C = \frac{1}{2} \int_0^{\infty} (\mathbf{x}^T Q_1 \mathbf{x} + \mathbf{u}^T Q_2 \mathbf{u}) d\tau$$

The controller performance index weights (the coefficients of  $Q_1$  and  $Q_2$ ) are purposely distributed in the continuous rather than in the discrete formulation. Indeed, the weighting matrices for the equivalent discrete cost function are computed according to an algorithm given by Bryson [9]; the equivalence relationship is necessary for coherent discretization using different sample periods. Besides, we chose to distribute the performance index weights such that the cross-track error is minimized and that drive motor saturation regions are avoided.

A steady-state discrete Kalman filter using CDGPS sensor inputs provides the basis for the predicted state estimation. In principle, optimal performance of the estimator requires that process and sensor noise be accurately modeled. In practice, this is often difficult to accomplish, and a trial and error process is typically used to empirically calibrate coefficients for these models. However, external disturbances can have different effects on the states depending on the vehicle's configuration, so a one-time tuning of disturbance models is not useful within the context of the integrated design process considered here. Therefore, we derive and implement detailed random process models in terms of vehicle design parameters.

To account for disturbances introduced by the non-flatness of the ground, we estimate the effects on the system states of a gravity vector, which is not perpendicular to the vehicle's plane, as illustrated Figure 3. The ground slope,  $\theta_G(t)$ , is assumed to be a correlated

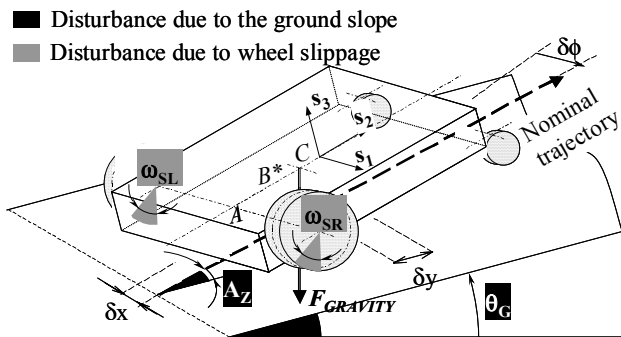


Figure 3 Process Noise Model

gaussian random function, and the azimuth of the slope with respect to the nominal trajectory,  $A_Z(t)$ , is uniformly distributed. A second source of disturbance results from the fact that rotations of the drive motor shafts do not necessarily generate a horizontal vehicle displacement, as in the case of a sudden obstacle, or of a loss of adherence on the wheels or on the reducers. Such disturbances are accounted for by assuming a random loss of angular velocity on the wheels and modeled with two gaussian random functions,  $\omega_{S\_R}(t)$  and  $\omega_{S\_L}(t)$  (see Figure 3). The derivation of the process noise vector is straightforward; for small values of  $\theta_G$ ,  $\omega_{S\_R}$  and  $\omega_{S\_L}$ :

$$\delta \mathbf{x} = G_d \mathbf{w}(t)$$

$$= \begin{bmatrix} -g \cos A_Z & 0 & 0 \\ (L_A - L_B) \frac{mg}{J_{ZZ}} \sin A_Z & 0 & 0 \\ 0 & 0 & 0 \\ 0 & R/2 & R/2 \\ 0 & -R/W & R/W \end{bmatrix} \begin{bmatrix} \theta_G(t) \\ \omega_{S\_R}(t) \\ \omega_{S\_L}(t) \end{bmatrix} \quad (14)$$

where  $G_d$  is the process noise input matrix, and  $\mathbf{w}(t)$  is the noise input vector. The spectral density for the continuous random process is obtained by calculating the expected value of  $\delta \mathbf{x} \cdot \delta \mathbf{x}^T$ . The equivalent covariance matrix in the discrete domain can be computed using an algorithm due to Van Loan [10], such that:

$$Q_d = \int_{T_s} e^{Ft} G_d R_w G_d^T (e^{Ft})^T dt, \quad (15)$$

where  $R_w$  is the random noise functions' spectral density matrix.

The sensor noise for the DGPS sensor is modeled by two gaussian random functions, noted  $v_{GPS\_x}(t)$  and  $v_{GPS\_y}(t)$ , for errors respectively in the  $x$  and  $y$  directions of the reference frame. Correlation due to multipath effects is modeled by a first order Markov process and estimated using state augmentation [11].

Both the discrete optimal LQR gain ( $K$ ) and the discrete Kalman prediction estimator gain ( $M$ ) are computed based on a discretized version of the state space representation (9), (10). The sample time used for the discretization is  $T_s$ , and corresponds to the sensor and actuator update rates. At this point of the process, parametric models for both the vehicle and the control system have been built, so that we can simulate their closed-loop trajectory-tracking performance as a function of relevant vehicle parameters.

## THEORETICAL SENSITIVITY ANALYSIS

At the climax of this work is the sensitivity analysis. We identify the effect of each system design parameter on the final path-following performance using a three-step process: covariance analysis to quantify performance sensitivity and bring the main trends into evidence; Monte-Carlo simulations (which use the full nonlinear vehicle model and take into account the effects of drive motor saturation) to confirm these results (next section); and experimental testing to provide the ultimate validation of the analysis and simulation results. Throughout the analysis, the trajectory-tracking performance index is chosen to be the standard deviation of the cross-track error on state  $x$ . A nominal configuration, defined at the bottom of Table 2, is used as reference for comparison when modifying parameters.

Covariance analysis provides immediate performance predictions over the whole range of variation of each parameter. The ensemble-average mean-square performance of the closed-loop system is estimated using discrete Lyapunov equations [10].

First, the results described in Section 3 are confirmed. Rows 2 and 3 of Table 2 show the losses in performance observed when driving “backward” and when selecting different motor windings (increasing  $R_a$ ,  $k_T$  and  $k_E$ ). We noted in Section 3 that these parameter modifications would make the open-loop poles less stable. Here we quantify the resulting effect on the closed-loop trajectory-tracking performance.

Then, there are several parameters for which we can anticipate the influence on the cross-track error, because of their obvious relationship to the system performance. For example, operating at lower nominal velocity ( $V_{y0}$ ) or

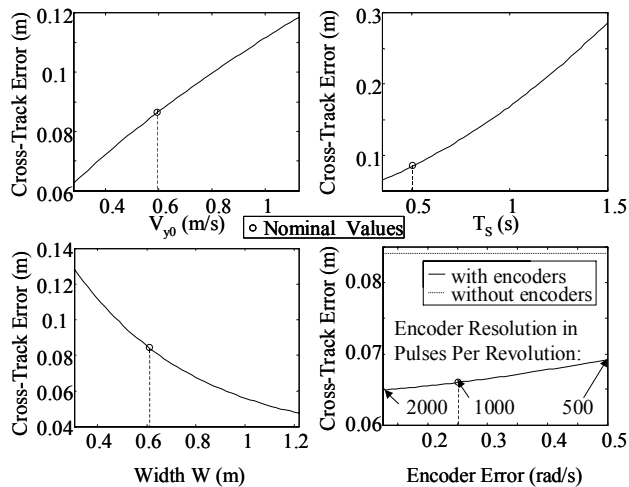


**Figure 4 Influence of Several Vehicle Parameters on the Path-Following Performance**

**Table 2 Summary of the Simulated and Experimental Results (standard deviations in cm)**

Configuration	Covariance	Monte-Carlo	Experiment
Nominal Case	8.4	9.8	6.7
Driving backward	8.5	10.0	
Increasing $R_a$ , $k_T$ , $k_E$	9.2	11.7	
Best Case ( $C=A$ , $S=front$ )	5.5	8.2	4.9
Worst Case ( $C=front$ , $S=back$ )	23.2	36.1	43.3
$T_S=1s$	16.9	20.0	20.1
With encoders	6.6	6.3	
Worst case, with encoders	16.6	16.7	15.2
Nominal: forward motion, $B^*$ , $S$ and $C$ in the center, $T_S=0.5s$			

at higher sample rate ( $1/T_S$ ) makes lateral trajectory corrections occur more frequently with respect to the distance traveled; a larger distance between the driving wheels ( $W$ ) increases the control sensitivity; and the addition of an auxiliary encoder sensor, described here for a range of resolution indexes, increases the accuracy of the state estimates. These trends are illustrated in Figure 4. The curves represent the cross-track error vs. variations in the parameter of interest. They also illustrate how we chose these parameters, after selection of the actual vehicle components on the industrial market.

Finally, one of the most valuable aspects of this sensitivity analysis, is that it unveils the sometimes complex relationship between final performance and vehicle parameters. In this case, we are interested in the performance impact of the locations of the control point ( $C$ ) and of the sensor point ( $S$ ). An immediate result is that the relative position of those two points matters for the final performance as illustrated on the three-dimensional curve Figure 5-c. Their individual impact can be studied by separating the “control performance”, which is a function of the location of  $C$  (Figure 5-a), and the “estimation performance”, which is a function of  $S$  (Figure 5-b).

The control performance is the average cross-track error obtained when assuming full-state feedback with a perfect sensor. Figure 5-a shows that the control performance is best when  $C$  is located on the driving axle ( $C$  and  $A$  coincident). The cross-track error increases slightly more rapidly as  $C$  is moved backward from  $A$  as opposed to forward from  $A$ . Classical control theory is useful to shed light on this problem. When studying the control performance (with full-state feedback), we can assimilate the vehicle to a single-input, single-output system, with  $u_L - u_R$  as input and  $x$  as output. The resulting transfer function is expressed as:

$$TF_x(s) = \beta' \frac{-L_A \cdot s + V_{y0}}{s^2 (s - \alpha')}$$

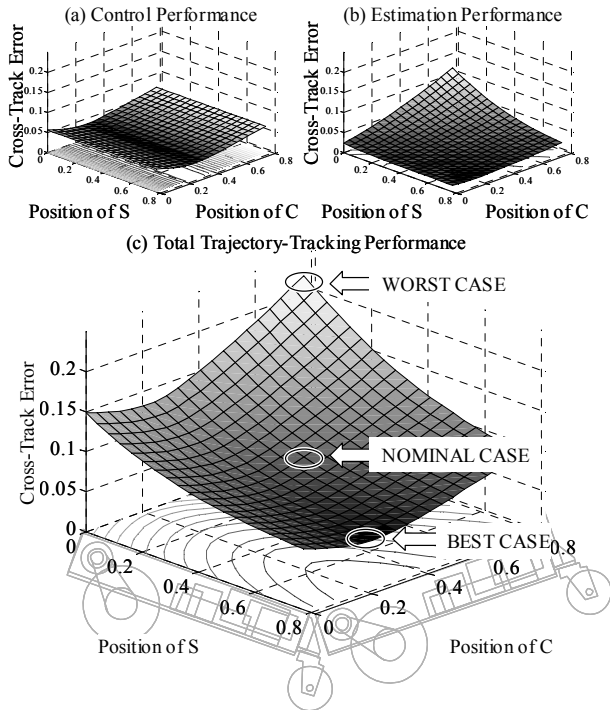


**Figure 5 Impact of  $S$  and  $C$  on the System Performance**

The three poles are independent of  $C$ , unlike the zero, which is equal to  $V_{y0}/L_d$  (where  $L_d$  is the signed distance from  $C$  to  $A$ ). We can study the associated root loci while  $C$  is moved along the vehicle. When  $C$  is in the back of  $A$ , nearly the entire root locus (two out of three branches) is in the right half of the complex plane. However,  $C$  being forward enough from  $A$ , the root locus is wholly in the left half plane. Therefore locating the control point in the front of the vehicle has a beneficial impact on control performance.

The estimation performance is given by the covariance of the Kalman filter's state estimate. Figure 5-b suggests that the antenna is best placed forward from the control point. Note that the variations in estimation performance are more significant in magnitude than the control performance.

The total trajectory-tracking performance is a combination of both control and estimation performances as suggested Figure 5-c. The best result is obtained with the antenna in the far front of the vehicle and the control point slightly forward of the driving axle. The worst configuration is with  $S$  in the back and  $C$  in the front. Between those two cases, more than 75% increase in performance is gained, which is most valuable given that there is almost no limiting mechanical constraint on the position of those two points. Notably, this increase in performance exceeds that provided by the additional use of encoder sensors with  $C$  and  $S$  at their worst case locations (see Table 2).

### MONTE-CARLO SIMULATIONS

When carrying out Monte-Carlo simulations, we can use a more complete model for the system, including nonlinearities, and therefore give a more reliable estimate of the final performance. Nevertheless, the process is time-consuming since it consists in estimating the ensemble-average vehicle path-tracking performance over numerous trials. Therefore only the main characteristics highlighted in the covariance analysis are simulated. The simulations are refined according to a parameter identification procedure, and further updated using experimental data.

A detailed block-diagram of the simulations is shown Figure 6. The controller is the same as in the covariance analysis. The reference input  $r_k$  is the output of an ideal

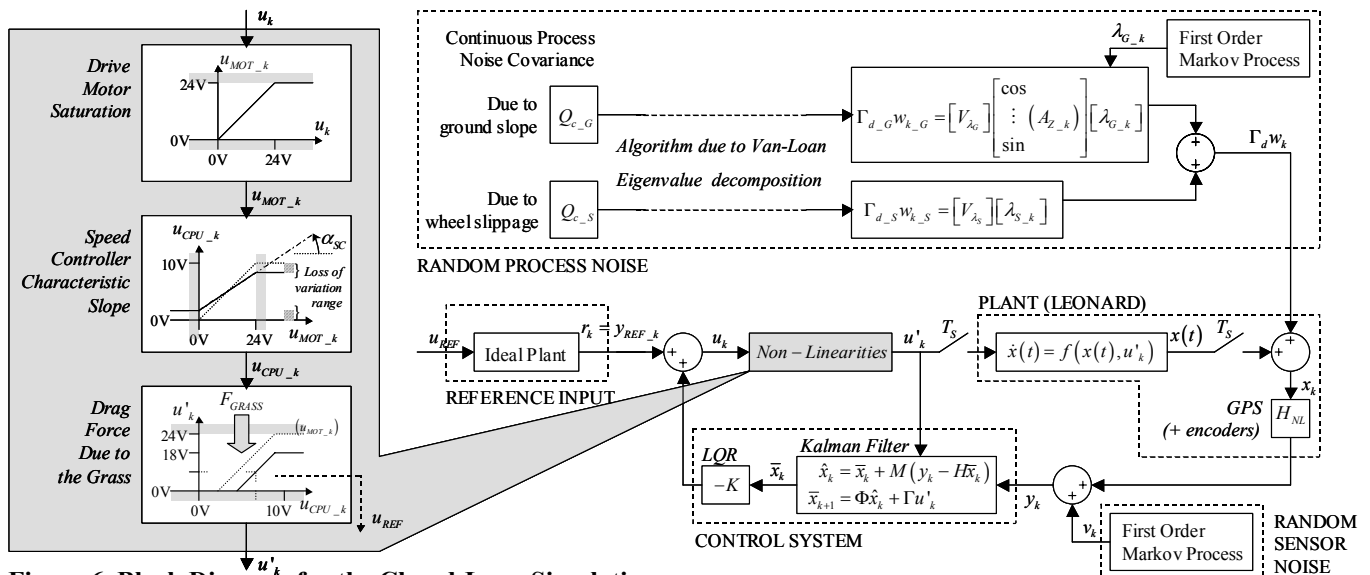


**Figure 6 Block Diagram for the Closed-Loop Simulations**

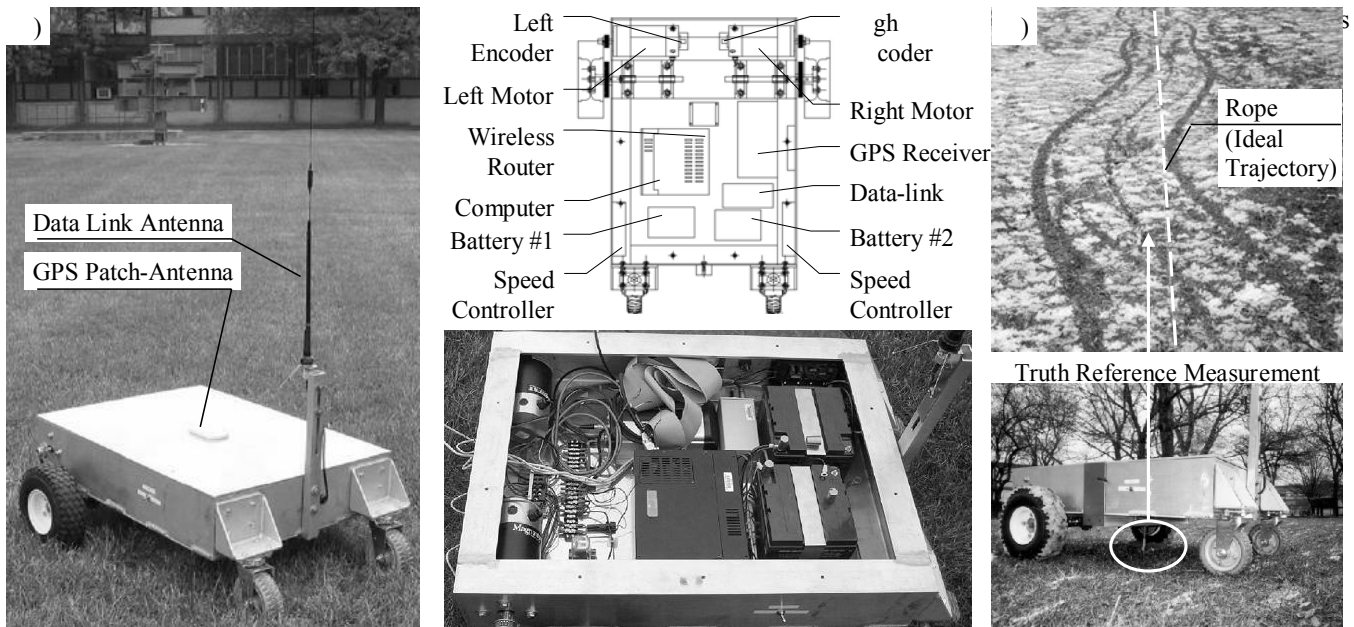


**Figure 7 (a) Final Vehicle Assembly and (b) Truth Reference Measurement**

plant operating at a nominal voltage  $u_{REF}$  (voltage necessary to operate at nominal velocity  $V_{y0}$ ). The nonlinearities due to the motors' saturation regions, the speed controller's characteristic slope and the grass' drag force (determined with the parameter identification procedure) are accounted for in the corrected input voltage  $u'_k$  to the plant. The continuous non-linear equations of motion for the vehicle (equations (1) to (8)) are numerically integrated over each sample period to model the behavior of the plant. Note that the derivation of the discrete-time random process noise vector  $\delta x_k$  requires more steps than for the covariance matrix (15). The complex calculations are not directly relevant to this discussion and therefore not described here. The sensor matrix  $H_{NL}$  is obtained from the non-linear equation (4) and (5).

With the Monte-Carlo simulations, the performance of the closed-loop system is predicted with a high degree of fidelity to the real physical system. The results of the simulations over 100 trials are given Table 2 (third column), and confirm the linearization hypotheses used for the covariance analysis. The differences with the covariance results stem from the added complexity in the Monte-Carlo simulations, in particular from the motor saturation.

## EXPERIMENTAL TESTING

The ultimate step of the sensitivity analysis is the experimental testing. Leonard has been tested in an open field after being designed according to the

In order to validate the results of the sensitivity analysis, we need to carry out a series of tests while physically modifying design parameters. Unfortunately this is not always possible. For example, the influence of motors' characteristics or of the frame's width cannot be tested with the available equipment, which explains why the last column of Table 2 is not totally filled up.

Truth reference position measurements are obtained by measuring, at regular intervals, the trace left in the snow by the vehicle with respect to an ideal linear trajectory, defined by a rope stretched in the North-South direction (Figure 7-b). In order to accurately observe the trajectory of the control point  $C$ , a pointing stick was fixed at  $C$  and left a trace for the point of interest.

For each configuration tested, we ran one 60 to 80m long trial at a nominal velocity ( $V_{y0}$ ) of 0.6m/s, and calculated the standard deviation of the lateral error. The results, given in Table 2 (fourth column), are consistent with the covariance analysis and the Monte-Carlo simulation results. Experimental and simulated trajectories for the nominal and worst configurations are presented for comparison Figure 8. Further calibration of simulation parameters would lead to a closer match between simulation and experiments, but the results are sufficiently accurate to highlight the desired trends. It is confirmed for example, that in the worst-case configuration, the cross-track deviation is more than 30cm, whereas in the optimal configuration, obtained by simply moving the GPS antenna, the error is less than 5cm.

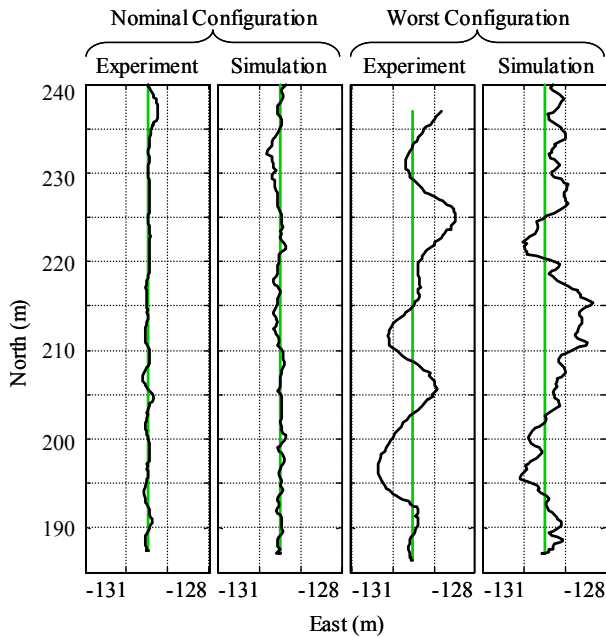


**Figure 8 Simulated and Experimental Trajectories**

For each configuration tested, we ran one 60 to 80m long trial at a nominal velocity ( $V_{y0}$ ) of 0.6m/s, and calculated the standard deviation of the lateral error. The results, given in Table 2 (fourth column), are consistent with the covariance analysis and the Monte-Carlo simulation results. Experimental and simulated trajectories for the nominal and worst configurations are presented for comparison Figure 8. Further calibration of simulation parameters would lead to a closer match between simulation and experiments, but the results are sufficiently accurate to highlight the desired trends. It is confirmed for example, that in the worst-case configuration, the cross-track deviation is more than 30cm, whereas in the optimal configuration, obtained by simply moving the GPS antenna, the error is less than 5cm.

### APPLICATION: AUTOMATED LAWNMOWER

An example of practical application of the previous design analysis is the use of Leonard as an automated lawnmower. The AGV described above constitutes the central unit carrying the power supply, navigation sensors, computation unit and providing motion. A standard off-the-shelf electric lawnmower is rigidly mounted to the AGV. This versatile modular design makes it easy to accommodate various sensors and tools, such as the mower or navigation sensors.

With the parametric controller derived in previous sections, modifications are easily applied to the model: the moment of inertia for the lawnmower is added to the initial model and the control point ( $C$ ) now designates the center of the cutting blades.

The control strategy for mowing a rectangular field takes advantage of the forward/backward motion capability of the vehicle. It aims to simply to go back and forth, straight along the field, each trip being offset by the width of the cutting blade, thus avoiding any turning maneuver.

With this strategy, it is desired not to favor one sense of motion at the expense of the other, so that the GPS antenna is located coincidentally with point  $C$ . Besides, two mounting options for the mower are available (in the front or in the back of the vehicle), which impact the positions of  $C$  and  $B^*$ . Analyses similar to the ones described above are carried out to select the solution that minimizes the trajectory-tracking error. Both  $C$  and  $B^*$  are best placed close to the driving axle,  $C$  for the reasons mentioned in previous sections (Figure 5-a), and  $B^*$  because the sensitivity of the system to external disturbances due to the ground slope increases as the distance between  $B^*$  and  $A$  increases (evident in the expression of  $G_d$  (14)). Therefore the mower is fixed in the back of the vehicle. The system was successfully tested in Chicago (Figure 9), and demonstrated cross-track control accuracy of less than 10 cm (standard deviation) at a nominal velocity of 2 km/hr.

In the light of these promising results, the Illinois Institute of Technology was an enthusiastic participant in last June's 'First Annual Autonomous Lawnmower Competition' sponsored and organized by the ION. In spite of some major last-minute challenges, we consider our involvement and our third place a great success.

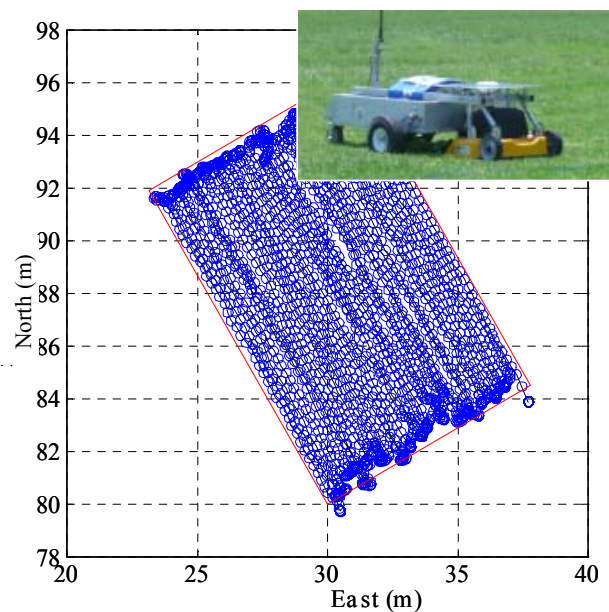


**Figure 9 Leonard Used as an Automated Lawnmower**

## CONCLUSION

In this work, we have demonstrated and quantified the impact on the trajectory-tracking performance, of vehicle design parameters such as the control point and GPS antenna locations. Careful selection of these parameters lead to performance improvements similar to that provided by the additional implementation of encoder sensors on the drive wheels. In addition to the Leonard mobile platform, a reliable and flexible high-fidelity simulation has been built and experimentally calibrated. Accurate predictions are therefore easily and immediately available for various AGV applications, as illustrated with the automated lawnmower.

## REFERENCES

- 1 O'Connor, M. (1997) *Carrier-Phase Differential GPS for Automatic Control of Land Vehicles*, PhD Thesis, Stanford University.
- 2 Bell, T. (1999) *Precision Robotic Control of Agricultural Vehicles on Realistic Farm Trajectories*, PhD Thesis, Stanford University.
- 3 Misra, P., Burke, B. P. and Pratt, M. M. (1999) 'GPS Performance in Navigation', *Proceedings of the IEEE*, Vol. 87, No. 1, pp. 65-85.
- 4 Opshaug, G. R. and Enge, P. (2000) 'Robotic Snow Cat', *Proceedings of ION GPS 2000 the 13<sup>th</sup> International Technical Meeting of The Satellite Division of The Institute of Navigation*, Salt Lake City, UT.
- 5 Hannu, M. (2001) *Outdoor Navigation of Mobile Robots*, PhD Thesis, The Finnish Academies of Technology, pp. 1-15, Finland.
- 6 Farrell, J. A., Han-Shue, T. and Yunchun, Y. (2003) 'Carrier Phase GPS-Aided INS-Based Vehicle Lateral Control', *Journal of Dynamic Systems, Measurement, and Control*, Transactions of the ASME, Vol. 125, pp. 339-353.
- 7 Christ, J. (2003) *Development of an Autonomous Ground Vehicle and Implementation of a GPS-Based Navigation System*, MS Thesis, Illinois Institute of Technology
- 8 Joerger, M. (2002) *Development of a GPS-Based Navigation and Guidance System for an Automated Ground Vehicle*, MS Thesis, Illinois Institute of Technology
- 9 Bryson, A. E. and Ho, Y.-C. (1975) 'Optimal Feedback Control', *Applied Optimal Control*, *Optimization, Estimation and Control*, Hemisphere Publishing Corp.
- 10 Bryson, A. E. (2002) *Applied Linear Optimal Control*, Cambridge University Press.
- 11 Gelb, A. (editor) (1974) 'Optimal Linear Filtering', *Applied Optimal Estimation*, The MIT Press.